High Angle of Attack Flight of a Subscale Aerobatic Aircraft

Or D. Dantsker,[*] and Michael S. Selig[†]

University of Illinois at Urbana–Champaign, Urbana, IL 61801

This paper describes initial high angle of attack flight testing performed by a subscale aerobatic aircraft. A 35% scale, 2.6 m (102 in) wingspan Sukhoi 29 S electric aircraft, the UIUC Subscale Sukhoi, was developed and used for this research. The aircraft was instrumented with a custom 100 Hz sensor data acquisition system, which had been previously developed and tested. The aircraft was flown through several stalls and descending harrier maneuvers during which flight data was recorded by the sensor data acquisition system. The flight data recorded during the maneuvers was used to produce time histories of aircraft state and aerodynamic coefficients. A brief literature review of similar aerobatic unmanned aircraft used for high angle of attack research is first presented. Then a background and a description of the development of the aircraft are given along with specifications. Next, information about data analysis methods used to analyze flight test data is given. After that, initial test flight results are presented, including flight path trajectory plots, time histories and aircraft aerodynamic coefficient data. Finally a list of proposed future work is given.

Nomenclature

ADC	=	analog-to-digital converters
$COTS$	=	commercial off the shelf
CG	=	center of gravity
DOF	=	degree of freedom
ESC	=	electronic speed controller
GPS	=	global positioning system
IMU	=	inertial measurement unit
PWM	=	pulse width modulation
RC	=	radio control
UAV	=	unmanned aerial vehicle
a_x, a_y, a_z =		body-axis translational acceleration
c	=	wing mean aerodynamic chord
C_D	=	drag coefficient ($D/\frac{1}{2}\rho V^2 S$)
C_L	=	lift coefficient ($L/\frac{1}{2}\rho V^2 S$)
C_M	=	moment coefficient ($M/\frac{1}{2}\rho V^2 Sc$)
D	=	drag
$\mathbf{F}$	=	force
I_{yy}	=	pitch moments of inertia
L	=	lift
M	=	pitching moment
m	=	aircraft mass
p, q, r	=	roll, pitch and yaw rates
S	=	wing area
u, v, w	=	body-fixed translational velocity
V	=	inertial speed

[*]Graduate Research Fellow, Department of Aerospace Engineering, AIAA Student Member. dantske1@illinois.edu
[†]Professor, Department of Aerospace Engineering, AIAA Associate Fellow. m-selig@illinois.edu

American Institute of Aeronautics and Astronautics

α	=	angle of attack
β	=	sideslip angle
$\phi,\ \theta,\ \psi$	=	roll, pitch and heading angles
ρ	=	density of air

I. Introduction

Exploring the aerodynamics of high angle of attack flight is becoming an ever more necessary task as more unmanned aerial vehicles (UAVs) are being developed with the ability to execute agile maneuvers. There have been lots of studies and modeling done related to high angle of attack aerodynamics.[1–6] However, due to the complexity and risk involved, there have only been a few testbeds that have actually taken flight and recorded experimental data.[7–11]

This paper describes high angle of attack flight testing performed by a subscale aerobatic aircraft, the UIUC Subscale Sukhoi, which is a 35% scale, 2.6 m (102 in) wingspan Sukhoi 29S electric aircraft, shown in Fig. 1. The aircraft is instrumented with a 100 Hz sensor data acquisition system based on the previously developed SDAC system.[12–14] The instrumented aircraft was flown through several high angle of attack maneuvers, stalls and descending harriers, during which flight data was recorded by the sensor data acquisition system. The flight data recorded during the maneuvers was used to produce flight path trajectory plots, time histories and aircraft aerodynamic coefficient data.

Figure 1. The UIUC Subscale Sukhoi aircraft.

The UIUC Subscale Sukhoi is able to perform aerodynamics research in the full-envelope flight regime, that is, over the full ±180 deg range in angle of attack and sideslip. The aircraft was developed based upon the experience gained from developing and operating the UIUC Aerotestbed.[10,15] The aircraft is equipped with a sensor data acquisition system to collect high-fidelity, high-frequency aircraft state data from takeoff to landing. The upgraded SDAC system features: a high-frequency, high-resolution six degree-of-freedom (6-DOF) inertial measurement unit (IMU) with a global positioning system (GPS) receiver, a pitot probe, a motor pulse tachometer, forty analog-to-digital converters, twelve pulse width modulation (PWM) control signal inputs, a down-link transceiver, and up to 64 GB of onboard storage. The system is able to record: 3D linear and angular accelerations, velocities, and position; airspeed, propeller rotation rate, control surface deflections, and control inputs, all at 100 Hz. The system also has the ability for further

American Institute of Aeronautics and Astronautics

expansion. The aerodynamic forces and moments, which are used to calculate the aerodynamic coefficients, are found by subtracting the thrust and gravitational force from the total forces and moments applied to the aircraft, which are measured by the IMU.

This paper will provide background and details about the development of the UIUC Subscale Sukhoi along with specification of the aircraft and the instrumentation system. Next will be a description of the flight test data analysis methods. After that, the results of the flight testing will be presented including time history plots of the aircraft trajectory, state and aerodynamic coefficients for each maneuver. Finally conclusions and future work will be discussed.

II.   Background, Development, and Specifications

The UIUC Subscale Sukhoi was developed based upon the experiences gained in developing and operating both the UIUC Aerotestbed used for spin and upset testing[10, 15] and the Avistar UAV used as a testing platform for the 100 Hz SDAC system.[12–14] As with the past systems, it was desired that the aircraft be able to log state data in all attitudes, thereby giving the aircraft the ability to perform aerodynamics research in the full-envelope flight regime, that is, over the full ± 180 deg range in angle of attack and sideslip.

The unmanned aircraft was built from a 35% scale, 2.6 m (102 in) wingspan Sebart Sukhoi 29S electric radio control model. The model aircraft airframe provides a light yet robust structure, which along with large control surfaces, allows the aircraft to perform aggressive aerobatic maneuvers. A photo of the un-assembled Sebart Sukhoi 29S 2.6m aircraft is given in Fig. 2. The aircraft was built using an electric propulsion system that uses a Hacker A150-8 motor and MasterSPIN 220 electronic speed controller, along with a Thunder Power 51.8 V, 10 Ah assembled lithium polymer battery pack. A diagram of the propulsion system is given in Fig. 3. The completed flight-ready aircraft physical specifications are given in Table 1, and its airframe component specifications are given in Table 2.
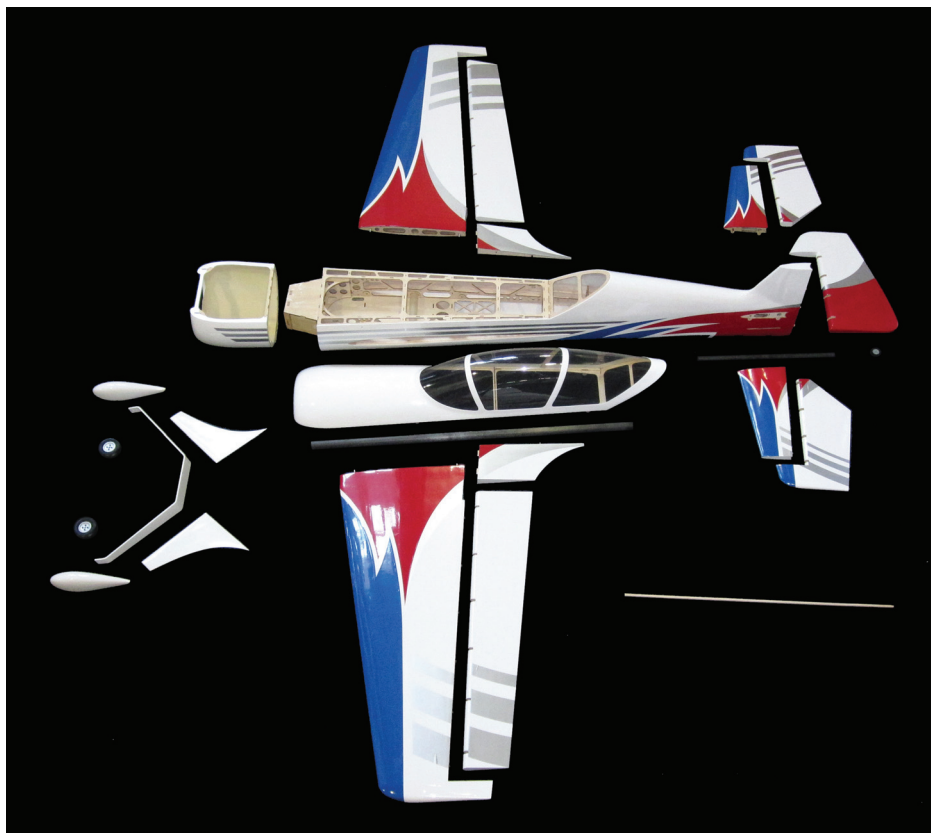
Figure 2. Sebart Sukhoi major airframe components with a 3 ft reference length placed on the bottom right.

American Institute of Aeronautics and Astronautics

Table 1. UIUC Subscale Sukhoi unmanned aircraft physical specifications

Geometric Properties	
Overall Length	100.0 in (2540 mm)
Wingspan	102.4 in (2600 mm)
Wing Area	2015 in^2 (130.0 dm^2)
Wing Aspect Ratio	5.20
Inertial Properties	
Weight	
Empty (w/o Batteries)	27.16 lb (12.33 kg)
14S 2P 10Ahr LiPo Main Battery	8.13 lb (3.69 kg)
RC and Avionics Batteries	0.77 lb (0.35 kg)
Gross Weight	36.00 lb (16.37 kg)
Wing Loading	41.2 oz/ft^2 (126 gr/dm^2)

Table 2. UIUC Subscale Sukhoi unmanned aircraft airframe component specifications

Construction	Built-up balsa and plywood structure, foam turtle decks, carbon fiber wing and stab tube, aluminum landing gear, fiberglass cowl, fiberglass wheel pants, and styrene and fiberglass canopy.
Flight Controls	
Control Surfaces	Ailerons (2), elevator (2), rudder, and throttle
Transmitter	Futaba T14MZ
Receiver	Futaba R6014HS
Servos	(8) Futaba BLS152
Power Distribution	SmartFly PowerSystem Competition 12 Turbo
Receiver Battery	Thunder ProLite RX 25c 2S 7.4V 2700 mAh
Propulsion	
Motor	Hacker A150-8 Outrunner
ESC	Hacker MasterSPIN 220
Propeller	Mejzlik 27x12TH
Motor Flight Pack	(4) Thunder Power ProPerformance 45c 7S 5000 mAh in 2S2P config.
Motor Power Switch	Emcotec SPS 120/240

American Institute of Aeronautics and Astronautics
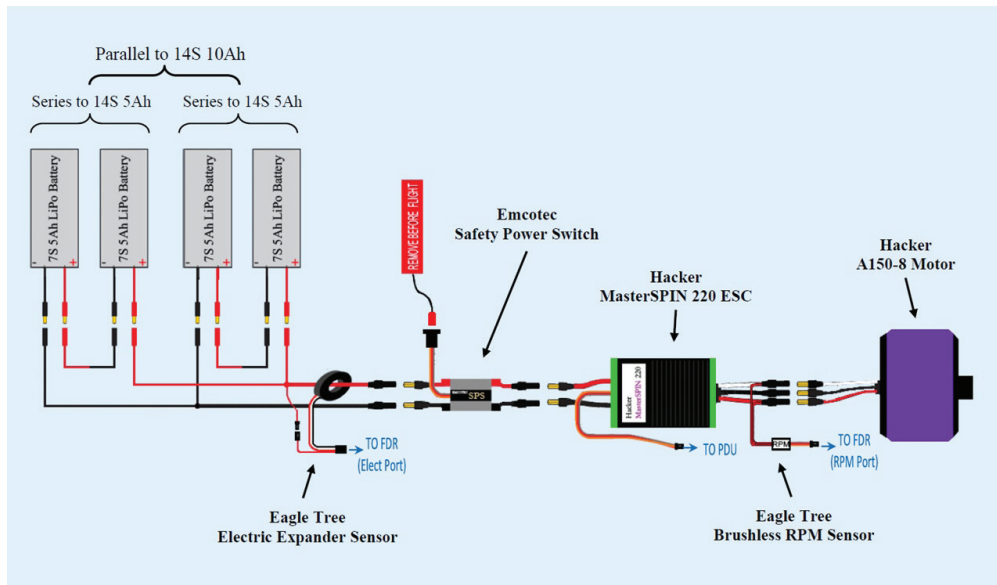
Figure 3. A propulsion system diagram for the UIUC Subscale Sukhoi unmanned aircraft

The aircraft was instrumented with an updated version of the custom sensor data acquisition system (SDAC),[12–14] which can be seen in Fig. 4. The SDAC was developed from COTS components and is plug-and-play, meaning that it could easily be installed into almost any aircraft. As mentioned earlier, the unit operates at 100 Hz and includes: a high-frequency, high-resolution six degree-of-freedom (6-DOF) inertial measurement unit (IMU) with a global positioning system (GPS) receiver, a pitot probe, an electronic tachometer, seven 10-bit analog-to-digital converters (ADC), thirty-two 12-bit analog-to-digital converters, a 14-bit analog-to-digital converter, twenty digital input/outputs (I/O), twelve pulse width modulation (PWM) signal inputs, a 40 mile downlink transceiver, an open serial, an open CANbus port, and up to 64 GB of onboard storage. Given the included sensors, the system is able to simultaneously log and transmit: 3D linear and angular accelerations, velocities, and position along with GPS location; pitot probe airspeed; 3D magnetic field strength and heading; control surface inputs; and control surface deflections. The performance specifications for the updated SDAC are given in Table 3. A description of the software architecture used in the implementation is given in Mancuso et al.[12]

The updated SDAC was fitted onto the aircraft and acts as the sensor data distribution hub for the various sensors installed. A system diagram depicting the specific configuration of the instrumentation, along with the flight control and propulsion systems, is shown in Fig. 5. Starting from the top-left of the diagram, the RC receiver outputs PWM control signals to servos and ESC, while a duplicate stream of PWM control signals are sent to the SDAC. The receiver gets its power from a Lipo battery connected through a regulator. The ESC, which drives the motor, draws power from its own battery. In the center of the diagram, the SDAC is connected to a variety of devices: an IMU, 3D magnetometer, 4 ADCs, an RPM sensor and a telemetry radio. Three of the ADCs are connected to potentiometers to measure control surface deflections while the last is used to measure the voltages of each of the batteries. The SDAC acquires data from the sensors and from the stream of PWM control signals coming from the receiver and outputs a unified stream to the telemetry radio while simultaneously logging it. The output stream can also be transmitted to another on-board device. The last two systems in the diagram are the telemetry radio and the video system, camera and transmitter, which can be added as desired. Each of these systems are powered by separate Lipo batteries with voltage regulators. As mentioned before, one of the ADCs is being used to measure the voltages of all the batteries. This ADC is connected to the raw output of each of the batteries through voltage dividers circuits that scale the voltages of the batteries to the range the ADC can measure. The specifications of the components used in the updated, tested sensor data acquisition system are given in Table 4 and information about the installation of these components is described in Dantsker et al.[13]
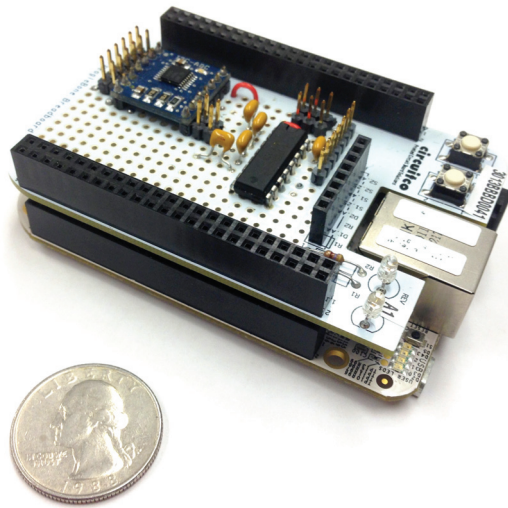
Figure 4. A photograph of the custom sensor data acquisition system (SDAC) unit.

Table 3. Updated sensor data acquisition (SDAC) system performance specifications

Sensors	
Inertial sensors	3-axis, ±18 g accelerometer 3-axis, ±300 deg/s gyroscope
Magnetometers	3-axis ±750 mG and 3-axis ±11 G
Altimeter (barometric)	1 ft resolution
Airspeed (pitot probe)	5–180 mph
GPS position	Up to 120 Hz (IMU assisted)
Tachometer	Up to 4 brushless motor pulse counters
Digital I/O	Up to 20
PWM inputs	Up to 12
Analog inputs	Up to 7x 10 bit, 32x 12 bit, 1x 14 bit
Further expansion capabilities	I2C, 1x serial port, CANbus
Data Handling	
Logging rate	100 Hz
Local output	Serial or Ethernet
Storage	Up to 64 GB microSD
RF link	40 mi
RF rate	10-25 Hz

American Institute of Aeronautics and Astronautics
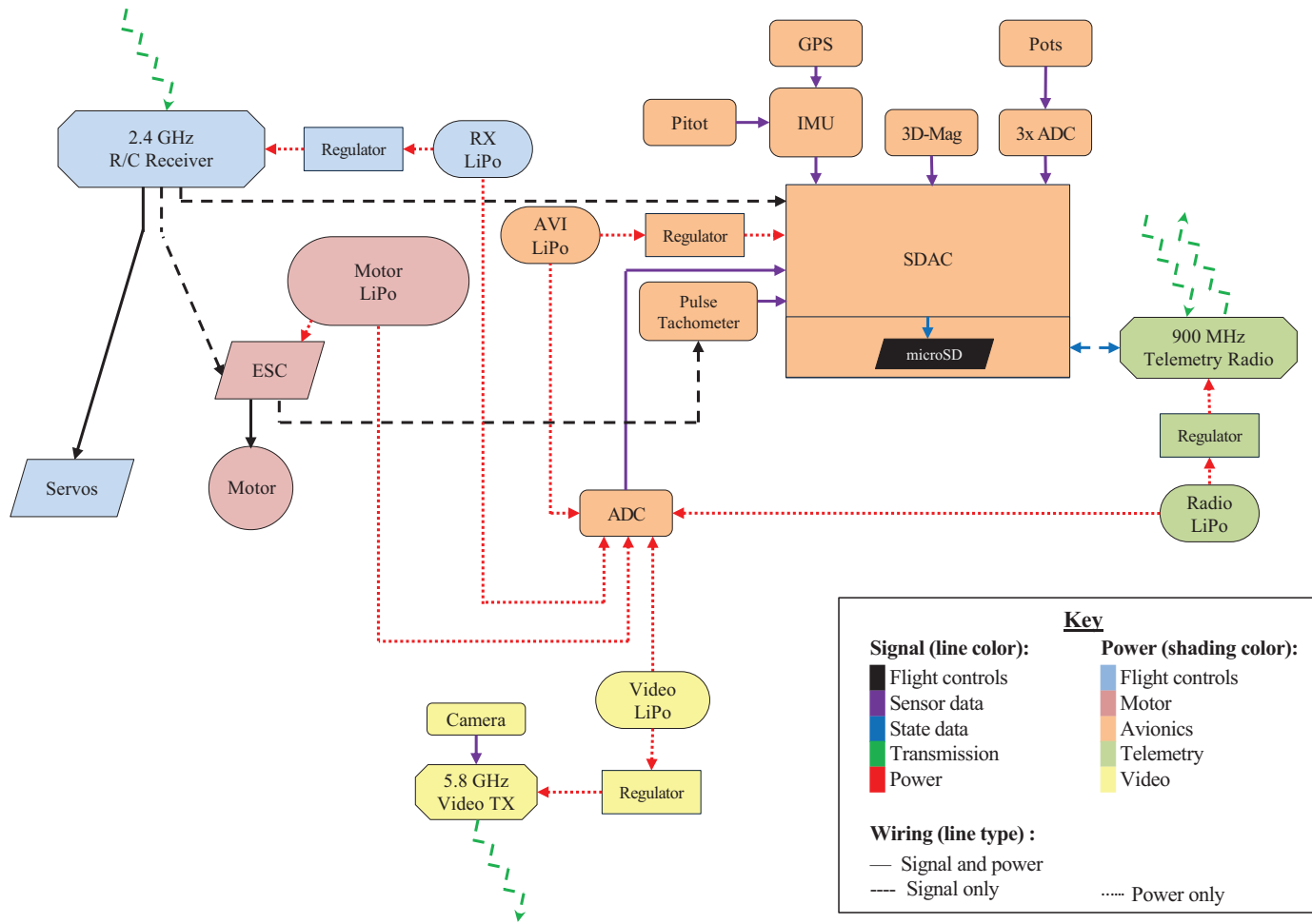
Figure 5. A block diagram of the aircraft systems.

Processing unit	BeagleBone running 32-bit Ubuntu Linux
Sensors	
IMU	XSens Mti-g 6-DOF IMU with Wi-Sys WS3910 GPS Antenna
Airspeed probe	EagleTree Systems pitot-static probe
Airspeed sensor	All Sensors 20cmH2O-D1-4V-MINI differential pressure sensor
Analog-to-digital converters	4x Gravitech 12 bit - 8 Channel ADC
Potentiometers	BI Technologies 6127
Tachometer	Sparkfun ProMicro
Power	
Regulators	Castle Creations CCBEC
Batteries	Thunder Power ProLite 3S 1350 mAh (avionics, telemetry and/or video)
Telemetry transceiver	Digi 9X Tend 900-MHz card
Data Storage	8GB microSD card

III. Data Analysis

Once sensor data is acquired by the SDAC, it needs to be post processed to produce meaningful results. The first, all corrupt values must be filtered out, which is done quite simply as the SDAC is programmed such that it produces an invalid value (e.g. -1 for a 12-bit integer (0-4095) field). Then in order to produce the aerodynamic coefficients, data from the IMU, pitot static probe and tachometer are used. The process follows the standard method to compute aerodynamic coefficients from flight data.[16] Effectively, the aerodynamic forces and moments, which are used to calculate the aerodynamic coefficients, are found by subtracting the forces and moments created by the propeller and the gravitational force from the total forces and moments applied to the aircraft, which are measured by the inertial measurement unit found on the aircraft.

The total external forces acting on the aircraft are a combination of the aerodynamic forces, thrust, and the gravitational force.

$$\mathbf{F}_{external} = \mathbf{F}_{aero} + \mathbf{F}_G + \mathbf{F}_T \tag{1}$$

By subtracting the gravitational force $\mathbf{F}_G$ and the thrust $\mathbf{F}_T$ from the total external forces, the aerodynamic forces can be found.

$$\mathbf{F}_{aero} = \mathbf{F}_{external} - \mathbf{F}_G - \mathbf{F}_T \tag{2}$$

where $\mathbf{F}_G$ is

$$\mathbf{F}_G = mg \left[-\sin\theta \quad \sin\phi\cos\theta \quad \cos\phi\cos\theta \right]^T \tag{3}$$

The total external forces acting on the aircraft can be found by multiplying the mass of the aircraft by the body-fixed axes accelerations (a_x, a_y, a_z), which are given by the IMU.

$$\mathbf{F}_{external} = \left[a_x \ a_y \ a_z \right]^T m \tag{4}$$

We define the body frame components of the aerodynamic force $\mathbf{F}_{aero}$ as (F_x, F_y, F_z). These components are transformed into the wind frame to yield expressions for lift and drag.

$$L = -F_z \cos\alpha + F_x \sin\alpha \tag{5a}$$
$$D = -F_z \sin\alpha \cos\beta - F_x \cos\beta \cos\alpha - F_y \sin\beta \tag{5b}$$

where α and β are

$$\alpha = \tan^{-1}(w/u) \tag{6a}$$
$$\beta = \sin^{-1}(v/V) \tag{6b}$$

The lift and drag coefficients are then found.

$$C_L = \frac{2L}{\rho V^2 S} \tag{7a}$$
$$C_D = \frac{2D}{\rho V^2 S} \tag{7b}$$

Given that the pitching moment is solely dependent on the aircraft, it can simply be found.

$$\mathbf{M} = I_{yy}\dot{q} \tag{8}$$

The moment coefficient is then found

$$C_M = \frac{2M}{\rho V^2 S c} \tag{9}$$

All required values are produced or can be derived from measurement taken by the IMU, pitot static probe and tachometer. For example, body frame accelerations and Euler angles are produced by the IMU, while the thrust is calculated from the airspeed and rotation rate given knowledge of the propeller's performance curves.

IV.   Initial Flight Test Results

The UIUC Subscale Sukhoi was flown fully-instrumented in the spring of 2015. During the flight testing, the aircraft was flown through several high angle of attack maneuvers, primarily (20 deg up elevator) stalls and descending harriers. These maneuvers provided a nice representation for the aircraft and instrumentation system capabilities while limiting the propeller modeling requirement to only a windmill drag model and a minimal-range thrust model. The motor would be kept 0% power for both maneuvers as to relieve the need for propeller modeling, which is quite demanding.[17] The data presented in the following discussion has not been filtered, with the exception of removing corrupt values as discussed earlier.

The stalls were performed by placing the aircraft in a powered climb and then powering off the motor. Just before the aicraft would enter stall, the elevators were deflected to a normal full deflection of 20 deg to aggravate the stall. A trajectory plot of a stall is given in Fig. 6 while a time history of the maneuver is given in Fig. 7. The lift, drag, and moment curves and the drag polar of the aircraft performing the stall are given in Fig. 8 and 9, respectively. It was assumed, and can be confirmed by the motor rotation rate time history that during the maneuver, the motor is still slowing down to a windmill brake state. Therefore the propeller was considered to be producing thrust, which is taken into account when computing the lift and drag coefficients. The time history of the stall shows an oscillation in the heading of the aircraft. The same oscillation is also visible in the roll rate, side slip velocity, and side slip velocity flow angle. The oscillation can likely be attributed to the aircraft experiencing high frequency wing rock, at approximately 4 Hz.

The time history of the lift coefficient shows a clear increase in lift as a result of the increase in angle of attack and quick deflection of the elevator. The time history of the drag coefficient, however, seems to lag the lift by approximately 2 sec, which can be reasoned by the fact that the dynamics of the aircraft are far faster than the flow separation. The lag in drag leads to a rather interesting drag curve where the drag coefficient stay approximately constant until about 2 sec and then increases rapidly as the aircraft angle of attack is starting to decrease. There also seems to be dynamic stall hysteresis evident for the lift, drag, and moment curve slopes. The result of this combination yields a rather odd drag polar.

Switching to the descending harrier, more dynamic effects will be visible. The descending harrier is performed by placing the aircraft in an unpowered glide and then pulling up on the elevator to hold the aircraft at a high angle of attack while descending, producing lots of drag from the exposed aircraft underside. A trajectory plot of a descending harrier is given in Fig. 10, while a time history of the maneuver is given in Fig. 11. The lift, drag, and moment curves and the drag polar of the aircraft performing the stall are given in Fig. 12 and 13, respectively. In this maneuver, it was assumed that the propeller was in a windmill brake state as the motor had been off for a significant amount of time and the RPM actually starts to increase as the aircraft accelerates downward. Therefore the propeller was considered to be producing drag, which is taken into account when computing the lift and drag coefficients.

The lift coefficient curve in Fig. 12 follows a typical constant slope until the point where the aircraft stalls and then experiences a hysteresis loop. This hysteresis loop is also visible on the drag coefficient curve. Similar to the stall, the descending harrier also seems to have a pretty constant drag coefficient, likely the result of some type of unsteady aerodynamic effects, where the separation again lags the dynamics of the aircraft The descending harrier produces a rather interesting drag polar, seen in Fig. 13, whereby the typical bucket is seen at the bottom; however, as it approaches what would be the top of the bucket, the aircraft quickly changes to a constant slope where the top of the bucket is typically located. The bucket also seems to have an exceptionally low lift-to-drag ratio, of less than one, which is assumed to be the result of the drag produced by the exposed aircraft underside.
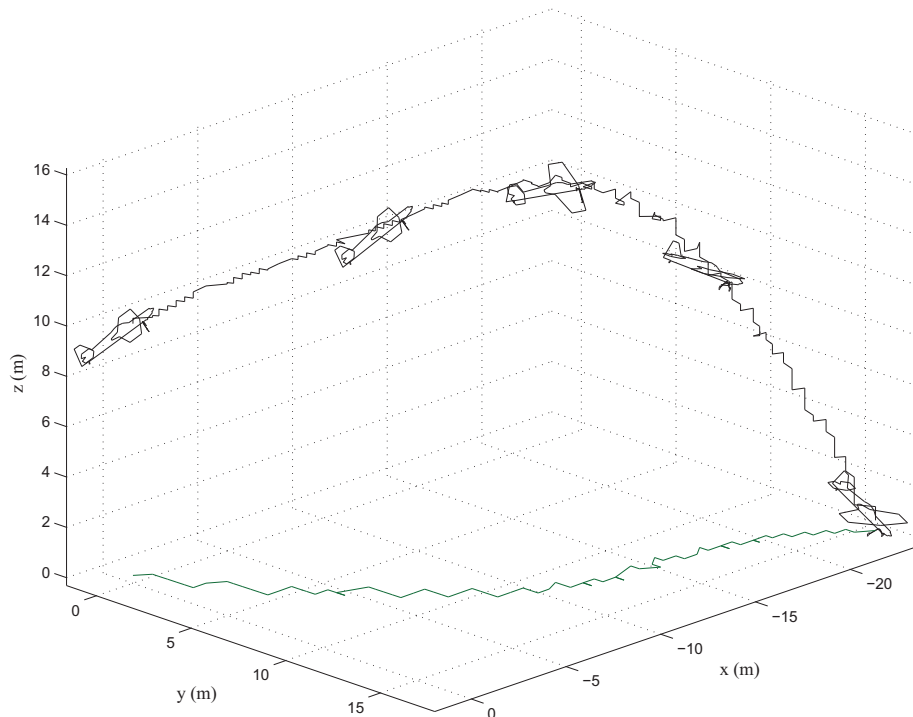
Figure 6. Trajectory plot of the stall (the aircraft is drawn two times larger than the actual size and once every second).

American Institute of Aeronautics and Astronautics
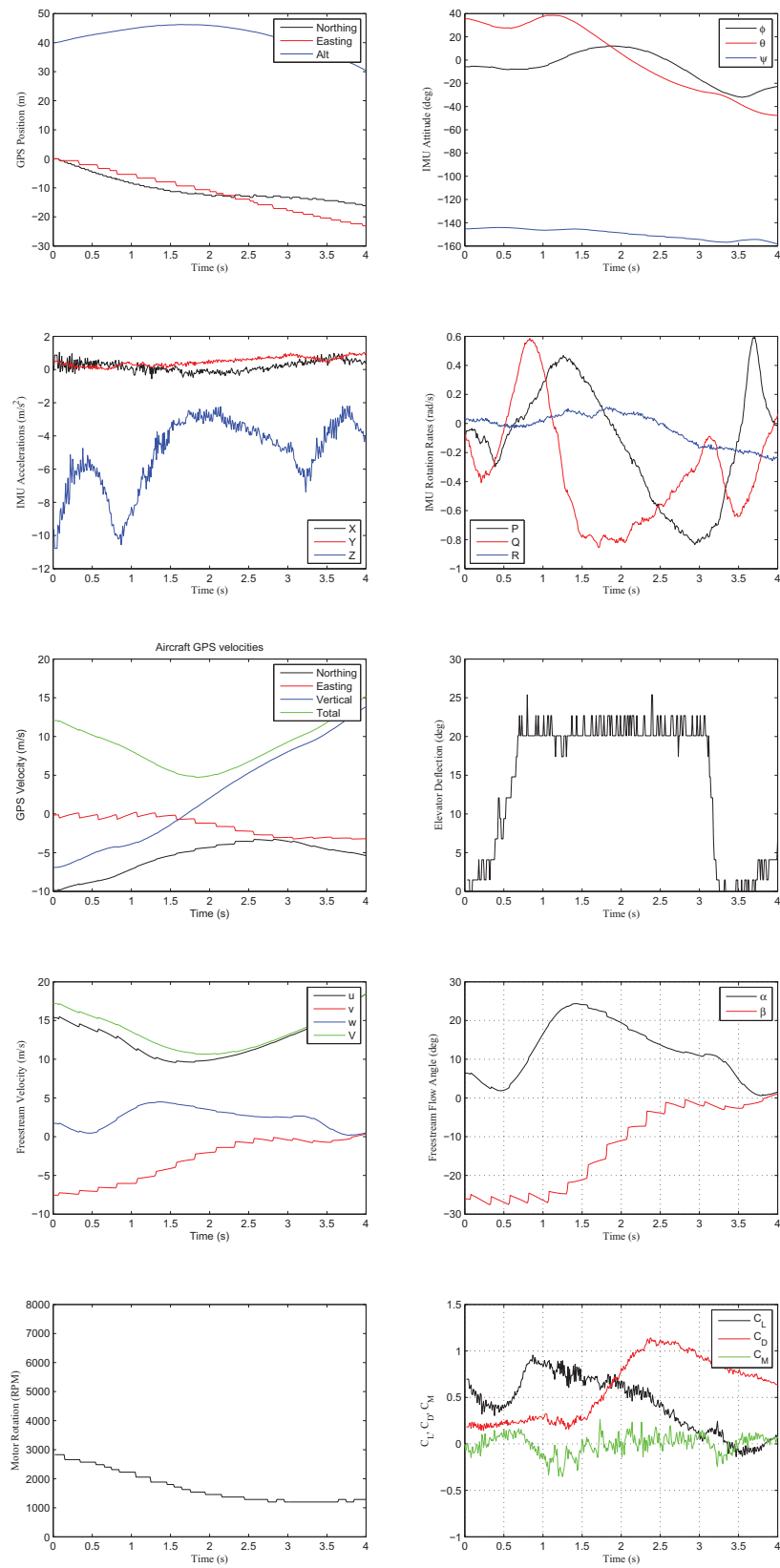
Figure 7. A time history of aircraft state during a stall.

American Institute of Aeronautics and Astronautics
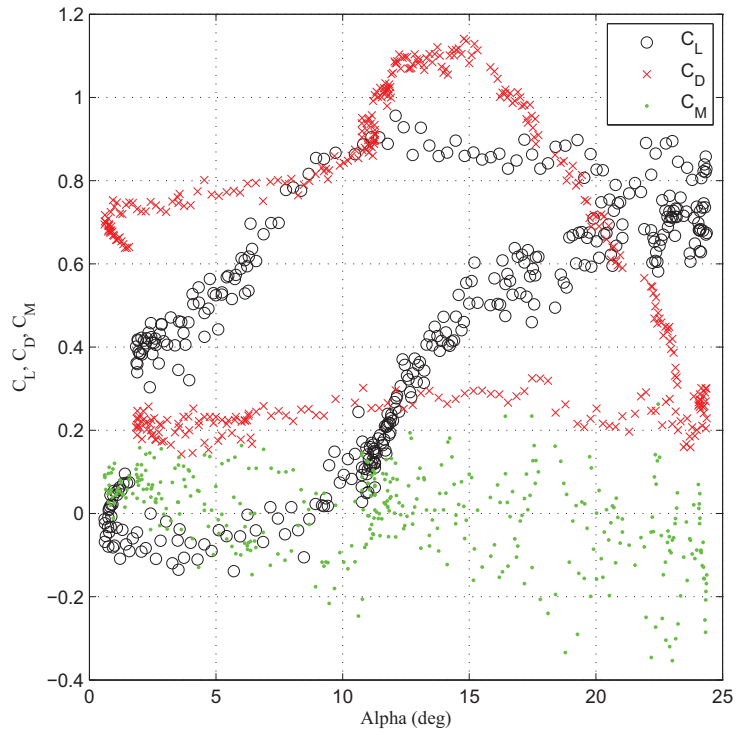
Figure 8. The lift, drag, and moment curves during the stall.
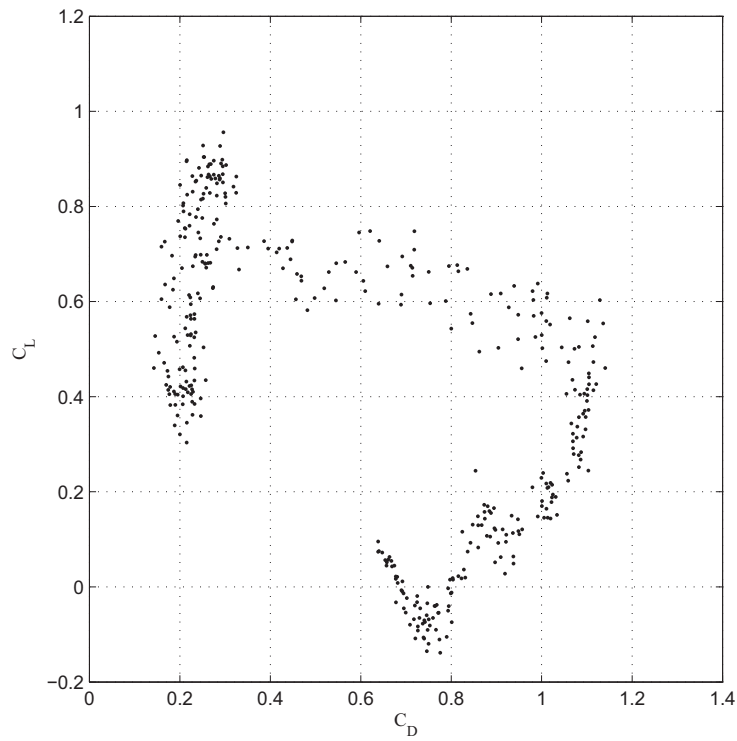
Figure 9. Drag polar during a stall.

American Institute of Aeronautics and Astronautics
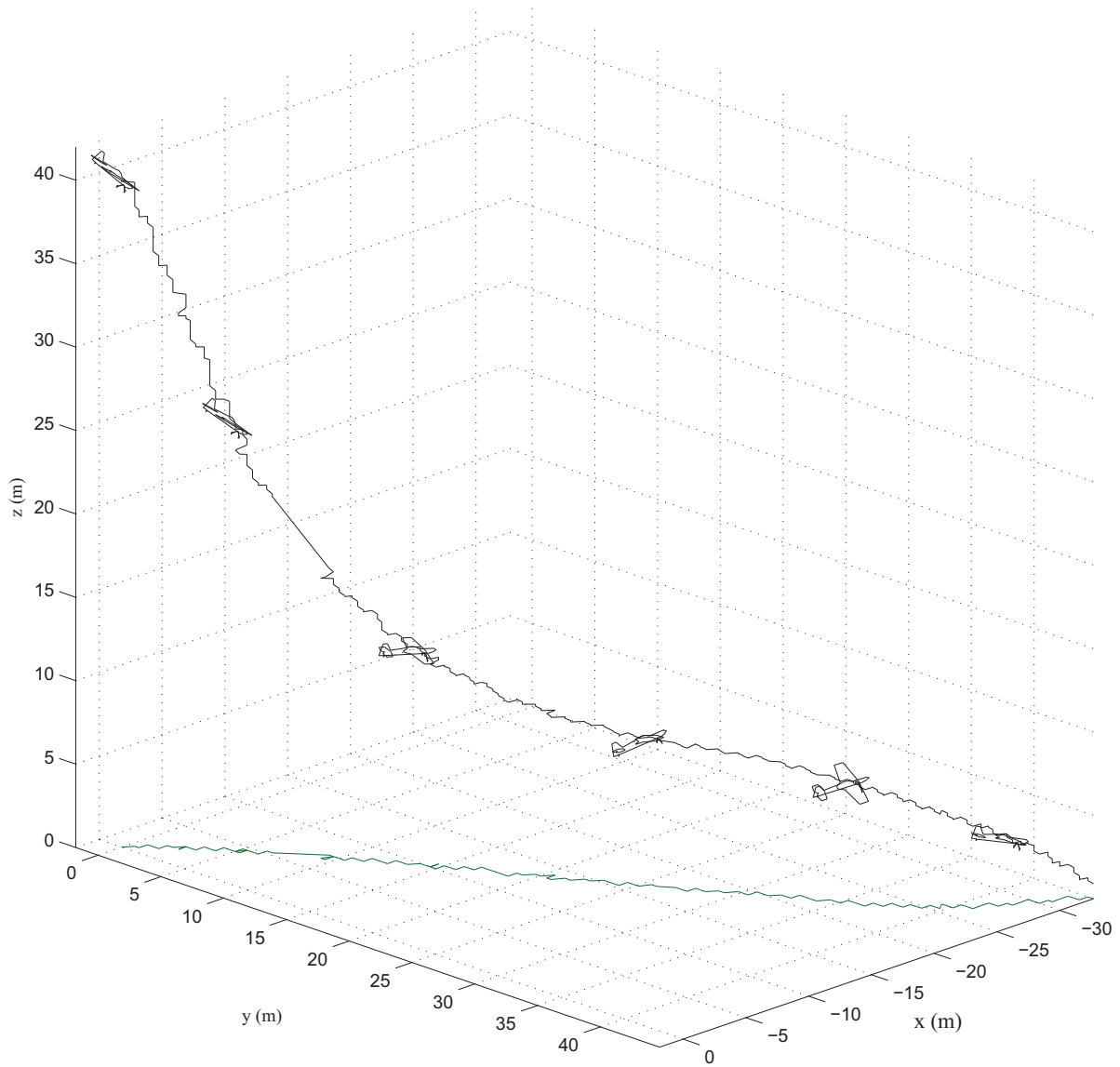
Figure 10. Trajectory plot of the descending harrier (the aircraft is drawn two times larger than the actual size and once every second).

American Institute of Aeronautics and Astronautics
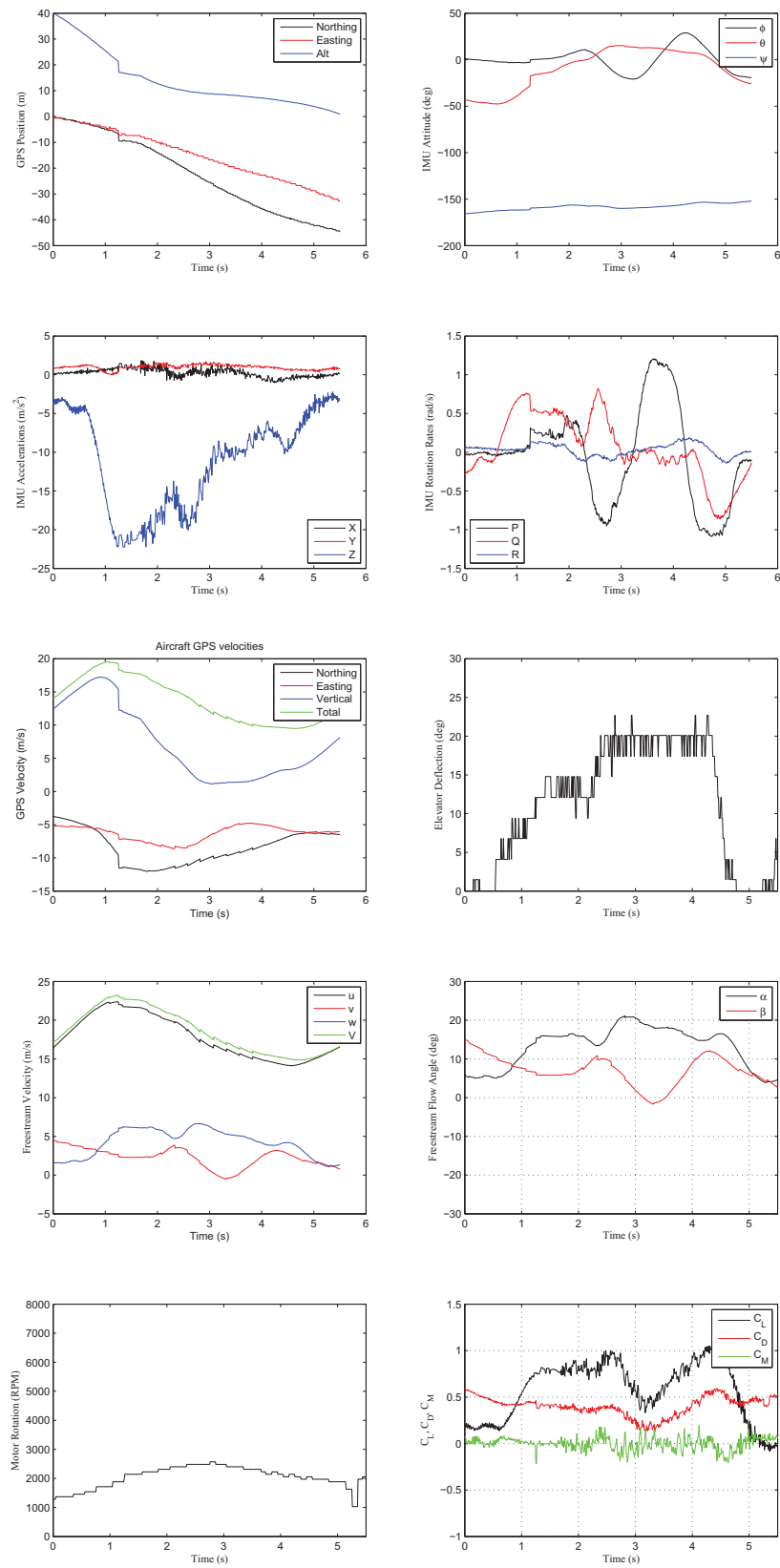
Figure 11. A time history of aircraft state during a descending harrier.

American Institute of Aeronautics and Astronautics
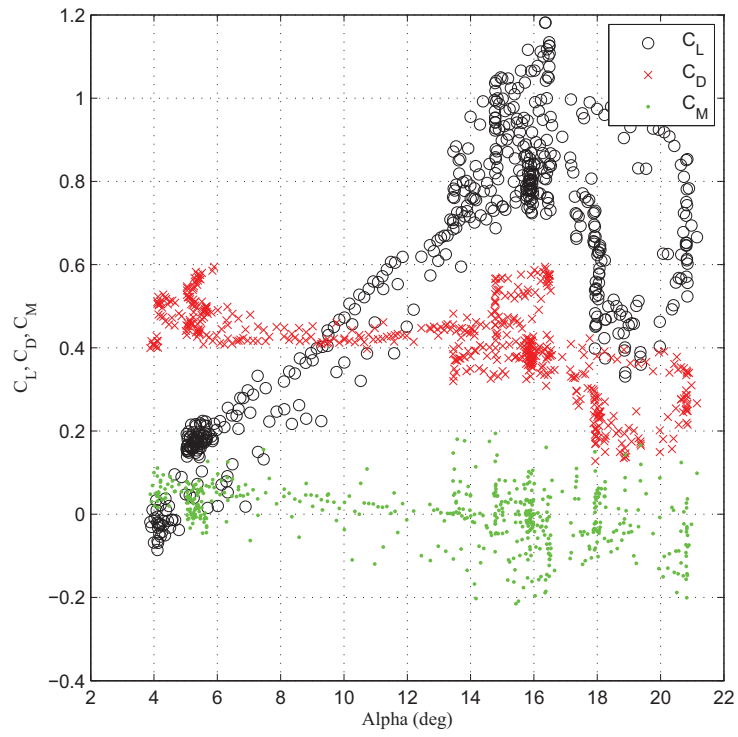
Figure 12. The lift, drag, and moment curves during the descending harrier.
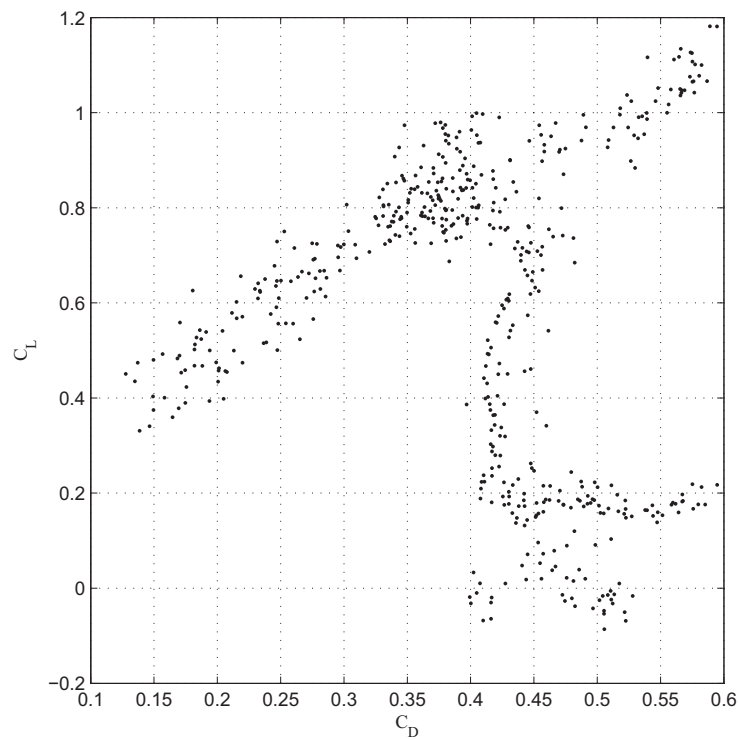
Figure 13. Drag polar during a descending harrier.

American Institute of Aeronautics and Astronautics

V.   Conclusions and Future Work

This paper described high angle of attack flight testing carried out using the UIUC Subscale Sukhoi, a 35% scale, 2.6 m (102 in) wingspan Sukhoi 29S electric aircraft, which was developed to perform aerodynamics research in the full-envelope flight regime. The aircraft is instrumented with a 100 Hz sensor data acquisition system and then flown through several high angle of attack maneuvers, specifically stalls and descending harriers, during which flight data was recorded. The flight data recorded was processed using analysis methods presented in the paper to produce flight path trajectory plots and rather interesting time histories and aerodynamic coefficient data, the result of unsteady aerodynamic effects exhibited by the aircraft. In the future, this unique flight testing platform will be leveraged in order to record flight data for a variety of other aerobatic maneuvers. More specifically, the aircraft will be used to perform maneuvers that both depart the linear flight regime and exhibit other unsteady aerodynamic effects.

Acknowledgments

Figure 14. The UIUC Subscale Sukhoi aircraft landing.

References

[1]McCroskey, W. J., "The Phenomenon of Dynamic Stall," NASA TM 81264, 1981.

[2]Goman, M. and Khrabrov, A., "State-Space Representation of Aerodynamic Characteristics of an Aircraft at High Angles of Attack," *Journal of Aircraft*, Vol. 31, No. 5, September–October 1994, pp. 1109–1115.

[3]Jouannet, C. and Krus, P., "Modelling of High Angle of Attack Aerodynamic State-Space Approach," *2006-3845*, AIAA Paper 2006-3845, AIAA Applied Aerodynamics Conference, San Francisco, CA, June 2006.

[4]Puopolo, M., Reynolds, R., and Jacob, J. D., "Comparison of Three Aerodynamic Models Used in Simulation of a High Angle of Attack UAV Perching Maneuver," No. 2013-0242, AIAA Paper 2013-0242, AIAA Aerospace Sciences Meeting, Grapevine, TX, June 2013.

[5]Sinha, M., Kuttieri, R. A., Ghosh, A. K., and Misra, A., "High Angle of Attack Parameter Estimation of Cascaded Fins Using Neural Network," *Journal of Aircraft*, Vol. 50, No. 1, January–February January 2013, pp. 272–291.

[6]Selig, M. S., "Real-Time Flight Simulation of Highly Maneuverable Unmanned Aerial Vehicles," *Journal of Aircraft*, Vol. 51, No. 6, November-December 2014, pp. 1705–1725.

[7]Cory, R. and Tedrake, R., "Experiments in Fixed-Wing UAV Perching," No. 2008-7256, AIAA Paper 2008-7256, AIAA Guidance, Navigation and Control Conference, Honolulu, HI, August 2008.

[8]Johnson, E. N., Wu, A. D., Neidhoefer, J. C., Kannan, S. K., and Turbe, M. A., "Test Results of Autonomous Airplane Transitions Between Steady-Level and Hovering Flight," *Journal of Guidance, Control, and Dynamics*, Vol. 31, No. 2, March-April 2008, pp. 358–370.

[9]Johnson, B. and Lind, R., "Characterizing Wing Rock with Variations in Size and Configuration of Vertical Tail," *Journal of Aircraft*, Vol. 47, No. 2, March-April 2010, pp. 567–576.

[10]Dantsker, O. D., Johnson, M. J., Selig, M. S., and Bretl, T. W., "Development of the UIUC Aero Testbed: A Large-Scale Unmanned Electric Aerobatic Aircraft for Aerodynamics Research," AIAA Paper 2013-2807, AIAA Applied Aerodynamics Conference, San Diego, California, June 2013.

[11]Uhlig, D. V., *Mico Air Vehicle Motion Tracking and Aerodynamic Modeling*, Ph.D. thesis, Dept. of Aerospace Engineering, University of Illinois, Urbana-Champaign, 2014.

[12]Mancuso, R., Dantsker, O. D., Caccamo, M., and Selig, M. S., "A Low-Power Architecture for High Frequency Sensor Acquisition in Many-DOF UAVs," International Conference on Cyber-Physical Systems, Berlin, Germany, Apr. 2014.

[13]Dantsker, O. D., Mancuso, R., Selig, M. S., and Caccamo, M., "High-Frequency Sensor Data Acquisition System (SDAC) for Flight Control and Aerodynamic Data Collection Research on Small to Mid-Sized UAVs," AIAA Paper 2014-2565, AIAA Applied Aerodynamics Conference, Atlanta, Georgia, June 2014.

[14]Dantsker, O. D., Loius, A. V., Mancuso, R., Caccamo, M., and Selig, M. S., "SDAC-UAS: A Sensor Data Acquisition Unmanned Aerial System for Flight Control and Aerodynamic Data Collection," Accepted to AIAA Infotech@Aerospace Conference, Kissimee, Florida, Jan 2015.

[15]Ragheb, A. M., Dantsker, O. D., and Selig, M. S., "Stall/Spin Flight Testing with a Subscale Aerobatic Aircraft," AIAA Paper 2013-2806, AIAA Applied Aerodynamics Conference, San Diego, CA, June 2013.

[16]Klein, V. and Morelli, E. A., *Aircraft System Identification: Theory and Practice*, AIAA Education Series, AIAA, Reston, VA, 2006.

[17]Selig, M. S., "Modeling Propeller Aerodynamics and Slipstream Effects on Small UAVs in Realtime," AIAA Paper 2010-7635, AIAA Atmospheric Flight Mechanics Conference, Toronto, Ontario, Canada, Aug. 2010.